Int J Mech Mater Des
DOI 10.1007/s10999-014-9241-6

Coupling of membrane element with material point method for fluid–membrane interaction problems

Yan-Ping Lian · Yan Liu · Xiong Zhang

Received: 6 December 2013 / Accepted: 7 January 2014

Abstract This paper proposes a coupled particle–finite element method for fluid–membrane structure interaction problems. The material point method (MPM) is employed to model the fluid flow and the membrane element is used to model the membrane structure. The interaction between the fluid and the membrane structure is handled by a contact method, which is implemented on an Eulerian background grid. Several numerical examples, including membrane sphere interaction, water sphere impact and gas expansion problems, are studied to validate the proposed method. The numerical results show that the proposed method offers advantages of both MPM and finite element method, and it can be used to simulate fluid–membrane interaction problems.

Keywords Material point method · Membrane element · Fluid–structure interaction · Contact method

1 Introduction

The fluid–membrane structure interaction has diverse engineering applications, such as vehicle airbags, printing presses, parachutes, blood vessels, bladder tanks, and so on. Due to large deformation of the membrane structure, the interaction between the membrane structure and the fluids is very strong, where a loose or weak coupling may be not adequate (Walhorn et al. 2005). Therefore, the development of robust and efficient numerical methods for strong fluid–membrane structure interaction problems still requires further research.

There are many methods for the fluid–structure interaction (FSI) problems, such as the coupling method between finite element method (FEM) and Eulerian methods, the arbitrary-Lagrangian Eulerian (ALE) method (Hughes et al. 1981; Souli et al. 2000) and the immersed boundary method (Luo et al. 2008). During recent years, significant efforts have been devoted to the development of particle methods, such as the smoothed particle hydrodynamics (SPH) method (Antoci et al. 2007; Rafiee and Thiagarajan 2009; Liu and Liu 2010), the natural neighbor Galerkin method (Daneshmand and Niroomandi 2007; Gonzalez et al. 2007), the material point method (MPM) (Sulsky et al. 1994; York II et al. 2000; Gan et al. 2011) and the particle finite element method (PFEM) (Idelsohn et al. 2004; Idelsohn et al. 2008). The particle methods describe the fluid and structure motion in the Lagrangian frame, so they are more convenient to track the fluid–solid interface and model the strong FSI problems than those methods based on the Eulerian frame. Furthermore, the particle methods have been coupled with FEM for FSI problems (Lee

Y.-P. Lian · Y. Liu · X. Zhang (✉)
School of Aerospace, Tsinghua University,
Beijing 100084, People's Republic of China
e-mail: xzhang@tsinghua.edu.cn

Published online: 18 January 2014

et al. 2007; Lian et al. 2011) to fully take their advantages.

The MPM (Sulsky et al. 1994) is a finite element method based particle method, which discretizes a material domain by a set of Lagrangian material points (particles). In MPM, the particles carry all state variables in order to model history-dependent materials; an Eulerian background grid is used to integrate the momentum equation and calculate space derivative. In each time step, the particles are rigidly attached to the Eulerian background grid and move with it. The kinematic variables are first mapped from particles to grid nodes to establish grid nodal momentum equations. Afterward, the solutions of the grid nodal momentum equation are mapped from the grid nodes back to the particles to update their positions and velocities. At the end of each time step, the deformed background grid is discarded and a new regular background grid is defined for the next time step. Hence, the difficulties associated with mesh distortion and element entanglement in FEM are fully eliminated, while numerical dissipation normally associated in Eulerian methods is reduced. York et al. (2000) employed MPM to simulate the 2D fluid–membrane structure interaction problem, where both the membrane and fluid are discretized by particles. In 2D problems, the membrane reduces to a curve line so that the normal vector can be obtained by the neighbor particles connection approximately. But in 3D problems, a special normal vector calculation scheme should be established. Gan et al. (2011) proposed an alternative method for the normal calculation, in which the membrane was discretized by a set of triangulares with the particles located at their vertices. The normal vector of each particle was determined by averaging the normal vector of all triangulares connected to the particle. By using this method, Gan et al. studied the zonal failure response in piezo-assisted intracytoplasmic sperm injection. Lian et al. (2011) proposed a coupled MPM–FEM method for FSI problems, in which the solid structure was modeled by hexahedral finite elements and the fluid by MPM particles.

The motivation of this work is to extend the capacity of MPM and membrane finite element to simulate the fluid–membrane interaction problems. Although MPM can be more accurate, more efficient and more robust than FEM for problems involving severe distortions, the accuracy of particle quadrature used in MPM is lower than that of Gauss quadrature used in FEM. Except that, MPM without further modification is not suitable to model the membrane structure directly (York II et al. 2000; Gan et al. 2011) for fluid–membrane interaction problems. So in this article, a method is presented for such problems, in which the membrane element (Hallquist 1998) is employed to model the membrane structure, while the MPM is employed to model the fluid. To take account of the strong interaction between fluid and membrane structures, a contact method (Bardenhagen et al. 2000; Huang et al. 2011; Hu and Chen 2003; Ma et al. 2010) is implemented, which is also used to couple two methods. The performance of the presented method is demonstrated by several numerical examples including membrane sphere interaction, water sphere impact and gas expansion problems.

The remaining part of this article is organized as follows. The governing equations for both fluid and membrane structure are given in Sect. 2, followed by MPM solution and membrane element in Sects. 3 and 4, respectively. The contact method for coupling MPM with membrane element is presented in detail in Sect. 5. The numerical implementation of the proposed method is summarized in Sect. 6, and aforementioned numerical examples are presented in Sect. 7. Finally, conclusions are given in Sect. 8.

2 Governing equation

In a material domain Ω, the governing equations in updated Lagrangian formulation are composed of mass conservation

$$\rho(\boldsymbol{X},t)J(\boldsymbol{X},t)=\rho_0(\boldsymbol{X}), \tag{1}$$

momentum conservation

$$\sigma_{ji,j}+\rho f_i=\rho\ddot{u}_i, \tag{2}$$

energy equation

$$\rho\dot{w}^{\text{int}}=D_{ij}\sigma_{ij}, \tag{3}$$

boundary conditions

$$\begin{cases}(n_j\sigma_{ij})\big|_{\Gamma_t}=\bar{t}_i\\ u_i|_{\Gamma_v}=\bar{u}_i\end{cases}, \tag{4}$$

and initial conditions

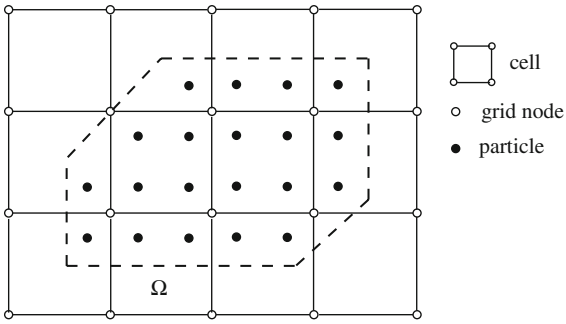

Fig. 1 MPM discretization

$$\begin{cases} \dot{u}(\boldsymbol{X},0) = \dot{u}_0(\boldsymbol{X}) \\ u(\boldsymbol{X},0) = u_0(\boldsymbol{X}) \end{cases}, \tag{5}$$

where ρ is the current density, J is the Jacobian determinant, $\boldsymbol{X}$ is the Lagrangian coordinate of a material point. Subscripts i and j denote the component of the space with Einstein summation convention, subscript 0 signifies the initial value, the comma denotes covariant differentiation, and the superimposed dot indicates the time derivatives. σ_{ij} is the Cauchy stress, f_i is the body force per unit mass, u_i is the displacement, D_{ij} is the rate-of-deformation, w is the internal energy per unit mass, and n_j is the unit outward normal to the boundary. Γ_t and Γ_u signify the prescribed traction boundary and displacement boundary of Ω, respectively.

Taking the virtual displacement δu_i as test function, the weak form of the momentum equation is obtained as

$$\begin{aligned} &\int_{\Omega} \rho \ddot{u}_i \delta u_i \mathrm{d}\Omega + \int_{\Omega} \sigma_{\mathrm{ij}} \delta \mathrm{u}_{\mathrm{i,j}} \mathrm{d}\Omega - \int_{\Omega} \rho \mathrm{f}_{\mathrm{i}} \delta \mathrm{u}_{\mathrm{i}} \mathrm{d}\Omega \\ &- \int_{\Gamma_{\mathrm{t}}} \mathrm{t}_{\mathrm{i}} \delta \mathrm{u}_{\mathrm{i}} \mathrm{d}\Gamma \\ &= 0, \end{aligned} \tag{6}$$

where the displacement boundary conditions are assumed to be satisfied as a priori.

3 MPM for fluid

3.1 MPM formulation

As shown in Fig. 1, MPM uses a set of particles to discretize the material domain. Due to mass lumped at each particle, density is approximated by Dirac delta function δ as

$$\rho(\boldsymbol{x}) = \sum_{p=1}^{n_p} m_p \delta(\boldsymbol{x} - \boldsymbol{x}_p), \tag{7}$$

where subscript p indicates the variable carried by particle p, n_p is the total number of particles, m_p and $\boldsymbol{x}_p$ are the mass and coordinate of particle p.

In MPM, particles are rigidly attached to the background grid in each time step as shown in Fig. 1. The kinematic information can be mapped between particles and grid nodes through the shape functions N_I. For 3D problem, the 8-point hexahedral cell is employed so that tri-linear shape functions are applied as follow

$$N_I = \frac{1}{8}(1+\xi\xi_I)(1+\eta\eta_I)(1+\zeta\zeta_I) \quad I = 1,2,\ldots,8, \tag{8}$$

where $\xi \in [-1,1]$, $\eta \in [-1,1]$ and $\zeta \in [-1,1]$ are the nature coordinates, ξ_I, η_I and ζ_I take on their nodal value of (± 1, ± 1, ± 1). The grid nodal momentum can be obtained by mapping particles momenta to the grid node, namely,

$$p_{iI} = \sum_{p=1}^{n_p} N_{Ip} m_p v_{ip}, \tag{9}$$

where the subscripts p and I denote variables associated with particle p and grid node I, respectively. $N_{Ip} = N_I(\boldsymbol{x}_p)$ is the value of shape function of grid node I evaluated at the site of particle p.

Substituting Eqs. (7) and (9) into Eq. (6) and invoking the arbitrariness of δu_{iI} lead to

$$\dot{p}_{iI} = f_{iI} \quad I = 1,2,\ldots,n_g \tag{10}$$

where

$$p_{iI} = m_I v_{iI} \tag{11}$$

is the nodal momentum of grid node I,

$$f_{iI} = f_{iI}^{\mathrm{ext}} + f_{iI}^{\mathrm{int}} \tag{12}$$

is the nodal force of grid node I,

$$f_{iI}^{\mathrm{int}} = -\sum_{p=1}^{n_p} N_{Ip,j} \sigma_{ijp} \frac{m_p}{\rho_p} \tag{13}$$

is the internal force,

Fig. 2 Time integration

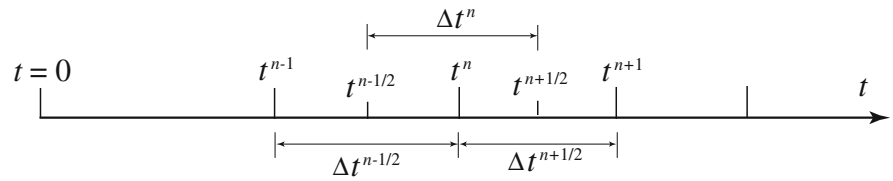

$$f_{iI}^{\text{ext}} = \sum_{p=1}^{n_p} N_{Ip}\bar{t}_{ip}h^{-1}\frac{m_p}{\rho_p} + \sum_{p=1}^{n_p} m_p N_{Ip} f_{ip} \tag{14}$$

is the external force, $\sigma_{ijp} = \sigma_{ij}(\boldsymbol{x}_p)$, $f_{ip} = f_i(\boldsymbol{x}_p)$, $\bar{t}_{ip} = \bar{t}_i(\boldsymbol{x}_p)$, and h denotes the thickness of the layer of the boundary.

In Eq. (11), the lumped mass matrix is used, namely

$$m_I = \sum_{p=1}^{n_p} m_p N_{Ip} \tag{15}$$

3.2 Time integration

The central difference time integration algorithm is used to integrate the momentum equation (12). Let $t^{n+1} = t^n + \Delta t^{n+1/2}$, $t^{n+1/2} = t^n + \Delta t^{n+1/2}/2 = t^{n-1/2} + \Delta t^n$ and $\Delta t^n = (\Delta t^{n-1/2} + \Delta t^{n+1/2})/2$, as shown in Fig. 2.

The momentum of grid node I at time $t^{n+1/2}$ is updated by

$$p_{iI}^{n+1/2} = p_{iI}^{n-1/2} + f_{iI}^n \Delta t^n, \tag{16}$$

where f_{iI}^n is the nodal force of grid node I, sum of nodal internal force and external force calculated by

$$f_{iI}^{\text{int,n}} = -\sum_{p=1}^{n_p} N_{Ip,j}^n \sigma_{ijp}\frac{m_p}{\rho_p} \tag{17}$$

$$f_{iI}^{\text{ext,n}} = \sum_{p=1}^{n_p} N_{Ip}^n \bar{t}_{ip}^n h^{-1}\frac{m_p}{\rho_p} + \sum_{p=1}^{n_p} m_p N_{Ip}^n f_{ip}^n \tag{18}$$

The position and velocity of particle p can be updated by the velocity and acceleration of grid node I at time $t^{n+1/2}$ and t^n, namely

$$x_{ip}^{n+1} = x_{ip}^n + \Delta t^{n+1/2}\sum_{I=1}^{n_g} p_{iI}^{n+1/2} N_{Ip}^n / m_I^n \tag{19}$$

$$v_{ip}^{n+1/2} = v_{ip}^{n-1/2} + \Delta t^n \sum_{I=1}^{n_g} f_{iI}^n N_{Ip}^n / m_I^n \tag{20}$$

The critical time step size is determined by

$$\Delta t = \min(L_e/c), \tag{21}$$

where L_e is the characteristic length of cell e, and c is the material local sound speed. The characteristic length L_e is constant in MPM because an Eulerian background grid with uniform cell is usually used in all time steps.

3.3 Stress update

In MPM, particle stresses are updated based on the Jaumann (co-rotational) stress rate σ_{ijp}^{∇}. Therefore, the material time derivative of the particle stress $\dot{\sigma}_{pij}$ is determined by

$$\dot{\sigma}_{ijp} = \sigma_{ijp}^{\nabla} + \sigma_{ilp}\Omega_{ljp} + \sigma_{jlp}\Omega_{lip}, \tag{22}$$

where the Jaumann stress rate σ_{ijp}^{∇} is determined from the strain rate $\dot{\varepsilon}_{ijp}$ by a constitutive model, and Ω_{ijp} is the spin tensor. Both the strain rate and spin tensor are calculated by

$$\dot{\varepsilon}_{ijp} = \frac{1}{2}\sum_{I=1}^{n_g}\left(N_{Ip,j}v_{iI} + N_{Ip,i}v_{jI}\right) \tag{23}$$

$$\Omega_{ijp} = \frac{1}{2}\sum_{I=1}^{n_g}\left(N_{Ip,j}v_{iI} - N_{Ip,i}v_{jI}\right) \tag{24}$$

The particle stress at time t^{n+1} is updated by

$$\sigma_{ij}^{n+1} = \sigma_{ij}^n + \dot{\sigma}_{ij}^{n+1/2}\Delta t^{n+1/2} \tag{25}$$

For hydrocodes, σ_{ij}^{n+1} is decomposed into deviatoric stress and pressure, which are updated with corresponding constitutive law and equation of state (EOS), respectively. As opposed to a solid point, the stress tensor for a compressible fluid point is given as

$$\sigma_{ij} = 2\mu\dot{\varepsilon}_{ij} - \frac{2}{3}\mu\dot{\varepsilon}_{kk}\delta_{ij} - p\delta_{ij}, \tag{26}$$

where μ is shear viscosity, and p is pressure which is usually determined from an EOS.

4 Membrane element

In FEM, the displacement u_i of a material point $\boldsymbol{X}$ within an element is approximated by

$$u_i(\boldsymbol{X},t) = \sum_{K=1}^{n_g} N_K(\xi(\boldsymbol{X}))u_{iK}(t), \tag{27}$$

where the subscript K denotes the FE nodes, n_g is the total number of nodes in the element, N_K is the shape function of node K. Taking quadrilateral elements as an example, the bilinear shape functions is

$$N_K = \frac{1}{4}(1+\xi\xi_K)(1+\eta\eta_K) \tag{28}$$

The integration over material domain in Eq. (6) can be calculated as the summation of the integration over all elements. Substituting Eq. (27) into Eq. (6) yields

$$\dot{p}_{iK} = f_{iK}^{\text{int}} + f_{iK}^{\text{ext}} \tag{29}$$

where

$$p_{iK} = m_K v_{iK}$$

is nodal momentum of FE node,

$$f_{iK}^{\text{int}} = -\sum_e \int_{V_e} N_{K,j}\sigma_{ji}dV$$

is the internal force of FE node,

$$f_{iK}^{\text{ext}} = \sum_e \left(\int_{V_e} \rho N_K f_i dV + \int_{\Gamma_{te}} N_K \bar{t}_i d\Gamma \right)$$

is the external force of FE node K.

For the sake of computational efficiency, one-point Gauss quadrature is used. Hence, the internal force and external force can be calculated by

$$f_{iK}^{\text{int}} = -\sum_e N_{Ke,j}\sigma_{jie}V_e \tag{30}$$

$$f_{iK}^{\text{ext}} = \sum_e \left(m_e N_{Ke} f_{ie} + \int_{\Gamma_{te}} N_K \bar{t}_i d\Gamma \right), \tag{31}$$

where subscript e denotes the value at the center of element e, and $m_e = \rho_e V_e$.

A membrane is a thin-walled structure that has stiffness only in the plane tangent to the structure and ideally no stiffness in bending. The stress components and traction through the thickness of a membrane are constant. The Belytschko membrane element (Hallquist 1998) is used to model the membrane structure. In the membrane element, the stresses are updated based on the combined co-rotational coordinates, which is embedded in and deform with the element.

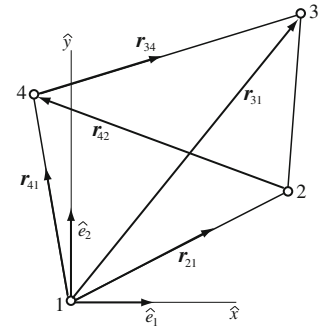

Fig. 3 Construction of element coordinate system

4.1 Co-rotational coordinates

The co-rotational coordinates are built based on the mid-surface of the quadrilateral element in terms of their nodal coordinates as shown in Fig. 3. The co-rotational coordinate system is embedded in and deforms with the element.

The procedure for constructing the coordinate system refers to DYNA3D code and begins by defining two tangent vectors $\boldsymbol{\chi}$ and $\boldsymbol{\psi}$ as

$$\boldsymbol{\chi} = \boldsymbol{r}_{21} + \boldsymbol{r}_{34} \tag{32}$$

$$\boldsymbol{\psi} = \boldsymbol{r}_{31} + \boldsymbol{r}_{42} \tag{33}$$

and then a unit vector normal to the two tangent vectors is determined by

$$\hat{\boldsymbol{e}}_3 = \frac{\boldsymbol{\chi}\times\boldsymbol{\psi}}{||\boldsymbol{\chi}\times\boldsymbol{\psi}||}, \tag{34}$$

where the superscript caret is used to indicate the local (element) coordinate system. To define the unit vectors $\hat{\boldsymbol{e}}_1$ and $\hat{\boldsymbol{e}}_2$, two auxiliary vectors, $\boldsymbol{\alpha}$ and $\boldsymbol{\beta}$, are defined as

$$\boldsymbol{\alpha} = \frac{\boldsymbol{\chi}+\boldsymbol{\psi}}{||\boldsymbol{\chi}+\boldsymbol{\psi}||} \tag{35}$$

$$\boldsymbol{\beta} = \frac{\hat{\boldsymbol{e}}_3\times\boldsymbol{\alpha}}{||\hat{\boldsymbol{e}}_3\times\boldsymbol{\alpha}||} \tag{36}$$

Finally, the unit vectors in the local $\hat{x}-\hat{y}$ coordinate system are obtained by

$$\hat{\boldsymbol{e}}_1 = \frac{1}{\sqrt{2}}(\boldsymbol{\alpha} - \boldsymbol{\beta}) \tag{37}$$

$$\hat{\boldsymbol{e}}_2 = \frac{1}{\sqrt{2}}(\boldsymbol{\alpha} + \boldsymbol{\beta}) \tag{38}$$

The transformation matrix $[q]$ between the global and local element coordinate systems is defined by the global components of the local coordinate system ($\hat{\boldsymbol{e}}_1$, $\hat{\boldsymbol{e}}_2$, $\hat{\boldsymbol{e}}_3$) as

$$[q] = \begin{bmatrix} e_{1x} & e_{2x} & e_{3x} \\ e_{1y} & e_{2y} & e_{3y} \\ e_{1z} & e_{2z} & e_{3z} \end{bmatrix}, \tag{39}$$

where e_{ix}, e_{iy}, e_{iz} are the global components of the element coordinate unit vectors. Using the matrix $[q]$, one can transform a vector from the local coordinate system to the global coordinate system, while using the matrix transpose $[q]^{\mathrm{T}}$ for the inverse transformation.

4.2 Strain rate

With one-point quadrature, the velocity–strain relations are evaluated only at the center of the mid-surface of the membrane by the standard bilinear shape function based on the co-rotational coordinates. The strain rate in the local $\hat{x} - \hat{y}$ plane at the element center (i.e. $\xi = 0$, $\eta = 0$) can be calculated as

$$\hat{D}_{\alpha\beta} = \frac{1}{2}\sum_{I=1}^{4}(N_{K,\beta}\hat{v}_{\alpha K} + N_{K,\alpha}\hat{v}_{\beta K}), \quad \alpha, \beta = 1, 2 \tag{40}$$

where

$$\hat{\boldsymbol{v}}_K = [q]^{\mathrm{T}}\boldsymbol{v}_K \tag{41}$$

is the nodal velocity of node K in the $\hat{x} - \hat{y}$ plane. Note that the strain rate components along $\hat{\boldsymbol{e}}_3$ are zero.

4.3 Nodal forces

After updating the stresses $\hat{\sigma}_{\alpha\beta}$ from the aforementioned strain rate by a suitable constitutive law, the local nodal internal forces can be obtained as

$$\hat{f}_{xK} = V\left(B_{1K}\hat{\sigma}^R_{xx} + B_{2K}\hat{\sigma}^R_{xy}\right) \tag{42}$$

$$\hat{f}_{yK} = V\left(B_{2K}\hat{\sigma}^R_{yy} + B_{1K}\hat{\sigma}^R_{xy}\right), \tag{43}$$

where V is the volume of the element, $B_{1K} = \frac{\partial N_K}{\partial \hat{x}}$, $B_{2K} = \frac{\partial N_K}{\partial \hat{y}}$. The global nodal internal force can be obtained by transforming the local internal nodal forces as

$$\begin{bmatrix} f_{xK} \\ f_{yK} \\ f_{zK} \end{bmatrix} = [q]\begin{bmatrix} \hat{f}_{xK} \\ \hat{f}_{yK} \\ 0 \end{bmatrix} \tag{44}$$

Therefore, the nodal internal forces Eq. (30) can be rewritten as

$$f^{\mathrm{int}}_{iK} = -\sum_e q_{ije}\hat{f}_{jKe}, \tag{45}$$

where the subscript e denotes the element.

Furthermore, the hourglass-resisting nodal force f^{Γ}_{iK} is calculated to control the hourglass modes induced by the one-point integration. Here, the Flanagan–Belytschko hourglass control scheme (Hallquist 1998; Flanagan and Belytschko 1981) is implemented.

4.4 Time integration

The central difference time integration algorithm is used to integrate the momentum equation. The nodal velocities at time $t^{n+1/2}$ are updated from Eq. (29) as

$$v^{n+1/2}_{iK} = v^{n-1/2}_{iK} + f^n_{iK}\Delta t^n / m_K \tag{46}$$

and the nodal positions at time t^{n+1} are updated by

$$x^{n+1}_{iK} = x^n_{iK} + v^{n+1/2}_{iK}\Delta t^{n+1/2} \tag{47}$$

The critical time step size is determined by

$$\Delta t = \min(L_e/c), \tag{48}$$

where L_e is the characteristic length of element e, and c is the material local sound speed. In order to keep all operations synchronic in the same loop, the minimum critical time step size of the FEM and MPM domains is used as the time step size.

5 Coupling scheme

The interaction between the fluid and the membrane structure is handled by a contact method implemented on a background grid. As shown in Fig. 4, the

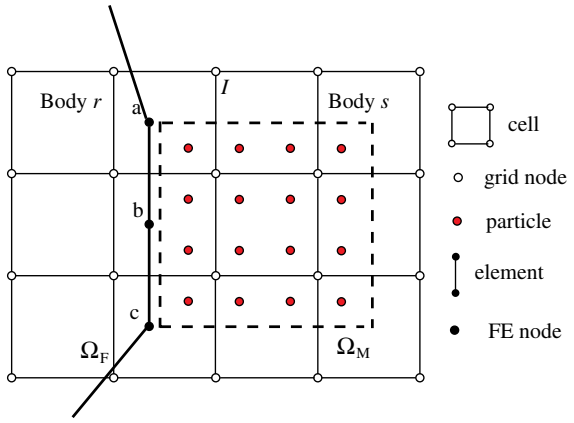

Fig. 4 2D illustration of coupling scheme

membrane body r, denoted by Ω_F, is modeled by FEM, while the fluid body s, denoted by Ω_M, is modeled by MPM. In each time step, the momentum equations of the MPM body and the FEM body are first updated independently to obtain trial solutions, as if they were not in contact. Then map the mass and momentum of FEM body to the background grid of MPM. If the momenta of the MPM body and the FEM body are projected to a same grid node, two bodies contact at the grid node, where a contact force is imposed on them to prevent penetration.

5.1 Contact detection

Let $\bar{p}_{iK}^{r,n+1/2}$ and $\bar{p}_{iI}^{s,n+1/2}$ denote the trial momentum of the FEM body r and the MPM body s, respectively. The trial velocity of grid node I contributed by bodies b can be obtained by

$$\bar{v}_{iI}^{b,n+1/2} = \frac{\bar{p}_{iI}^{b,n+1/2}}{m_I^{b,n}}, \quad b = r, s \tag{49}$$

where

$$m_I^{b,n} = \sum_p m_p^{b,n} N_{Ip}, \quad b = r, s$$

is the grid nodal mass contributed by body b. If

$$(\bar{v}_{iI}^{r,n+1/2} - \bar{v}_{iI}^{s,n+1/2}) n_{iI}^{r,n} > 0 \tag{50}$$

two bodies may penetrate each other in the vicinity of grid node I. In Eq. (24), $n_{iI}^{r,n}$ is the unit outward normal of body r at point I. In the FEM domain Ω_F, $n_{iI}^{r,n}$ equals to the summation of normal vectors of the element mid surface, while in the MPM domain Ω_M, $n_{iI}^{s,n}$ can be obtained by the gradient of the particles mass (Bardenhagen et al. 2000) as

$$n_{iI}^{s,n} = \sum_p N_{Ip,i}^n m_p \tag{51}$$

In order to avoid numerical singularity, Eq. (50) can be rewritten in the momentum form by multiplying $m_I^{r,n} m_I^{s,n}$ as

$$(m_I^{s,n} \bar{p}_{iI}^{r,n+1/2} - m_I^{r,k} \bar{p}_{iI}^{s,k+1/2}) n_{iI}^{r,n} > 0 \tag{52}$$

Contact detection based on Eq. (52) may cause false contact, hence the improved contact detection method proposed by Ma and Zhang et al. (2010) is used, in which the real distance between two bodies is calculated to assist the contact detection.

5.2 Contact force

If two bodies contact at grid node I, a contact force $f_{iI}^{b,c,k}$ must be imposed at the grid node to prevent penetration. Then the real momentum $p_{iI}^{b,n+1/2}$ of body b at grid node I can be obtained by

$$p_{iI}^{b,n+1/2} = \bar{p}_{iI}^{b,n+1/2} + \Delta t^n f_{iI}^{b,c,n} \tag{53}$$

For stick contact, the real momentum $p_{iI}^{b,n+1/2}$ must satisfy the impenetrability condition

$$(m_I^{s,n} p_{iI}^{r,n+1/2} - m_I^{r,n} p_{iI}^{s,n+1/2}) n_{iI}^{r,n} = 0 \tag{54}$$

namely, $(v_{iI}^{r,n+1/2} - v_{iI}^{s,n+1/2}) n_{iI}^{r,n} = 0$, which indicates the continuity of velocity on the contact interface. Substituting Eq. (53) into Eq. (26) gives the stick contact force

$$f_{iI}^{r,c,n} = -f_{iI}^{s,c,n} = \frac{m_I^{s,n} \bar{p}_{iI}^{r,n+1/2} - m_I^{r,n} \bar{p}_{iI}^{s,n+1/2}}{(m_I^{r,n} + m_I^{s,n}) \Delta t} \tag{55}$$

which indicates the continuity of normal acceleration on the contact interface. The normal contact force $f_I^{\text{nor},k}$ and the tangential contact force $f_{iI}^{b,\tan,k}$ are given by

$$f_I^{\text{nor},k} = f_{jI}^{b,c,n} n_j^{b,n} \tag{56}$$

$$f_{iI}^{b,\tan,k} = f_{iI}^{b,c,n} - f_I^{\text{nor,n}} n_i^{b,n} \tag{57}$$

For slip contact, the tangential contact force is limited to $\mu f_I^{\text{nor,n}}$ based on Coulomb friction model, where μ is the friction coefficient. Therefore the contact force is rewritten as

$$f_{iI}^{b,c,n} = f_I^{\text{nor,n}} n_i^{b,n} + \mu f_I^{\text{nor,n}} \left| \frac{f_{iI}^{b,\text{tan,n}}}{|f_{iI}^{b,\text{tan,n}}|} \right| \tag{58}$$

For the MPM body, the real nodal momentum is obtained by Eq. (53). For the FEM body, the real nodal velocity is obtained by the background grid nodal acceleration as

$$v_{iK}^{n+1/2} = \bar{v}_{iK}^{n+1/2} + \Delta t^n \sum_{I=1}^{n_g} f_{iI}^{b,c,n} N_{Ip}^n / m_I^n \tag{59}$$

The position of finite element nodes can be updated based on the updated nodal velocity.

6 Numerical implementation

The detailed implementation of the method is presented as follows:

1. Initialize the background grid, and reset all grid nodal variables to zero.
2. Calculate the trial solution of the MPM body on the background grid

(a) Loop over all the particles in the MPM body s to calculate their contributions to the masses and the momenta of grid nodes by

$$m_I^{s,n} = \sum_p^{n_p} m_p^s N_{Ip}^n \tag{60}$$

$$p_{iI}^{s,n-1/2} = \sum_p^{n_p} m_p^s v_{ip}^{s,n-1/2} N_{Ip}^n \tag{61}$$

(b) Apply the essential boundary conditions on the background grid nodes. If the node I is fixed in i direction, set $p_{iI}^{s,n-1/2} = 0$.

(c) Loop over all particles to calculate their incremental strains and spin tensors, respectively, by

$$\Delta\varepsilon_{ijp}^{n-1/2} = \frac{1}{2}\Delta t^n \sum_{I=1}^{8} \left[N_{Ip,j}^n v_{iI}^{s,n-1/2} + N_{Ip,i}^n v_{jI}^{s,n-1/2} \right] \tag{62}$$

$$\Omega_{ijp}^{n-1/2} = \frac{1}{2} \sum_{I=1}^{8} \left[N_{Ip,j}^n v_{iI}^{s,n-1/2} - N_{Ip,i}^n v_{jI}^{s,n-1/2} \right] \tag{63}$$

The stresses of particles can be updated by corresponding constitutive law and EOS.

(d) Loop over all the particles to calculate the grid nodal internal forces $f_{iI}^{\text{int},n}$ and external forces $f_{iI}^{\text{ext},n}$ by using Eqs. (17) and (18), respectively.

(e) Loop over all the background grid nodes to update their trial momenta by

$$\bar{p}_{iI}^{n+1/2} = p_{iI}^{n-1/2} + \Delta t^n f_{iI}^n \tag{64}$$

and apply the essential boundary conditions. If the node I fixed in i direction, set $f_{iI}^n = 0$.

3. Calculate the trial solution of the FEM (membrane element) body

(a) Loop over all the elements to calculate their co-rotational coordinates and transformation matrix by Eq. (39).

(b) Transform the nodal velocities $v_{iI}^{r,n-1/2}$ to the local coordinate system by Eq. (41).

(c) Calculate the strain rate at element center by Eq. (40), the nodal internal forces $f_{iK}^{\text{int},n}$ by Eq. (45), the nodal external forces $f_{iI}^{\text{ext},n}$ by Eq. (31) and the hourglass resisting forces.

(d) Apply the essential boundary condition. If the node K is fixed in i direction, set $f_{iK}^n = 0$.

(e) Loop over all the FE nodes to update their trial velocities by Eq. (46).

4. Contact detection and treatment

(a) Map the nodal mass and momentum of the FEM body to the background grid.

(b) Loop over all the grid nodes to detect the contact grid nodes. If Eq. (52) is satisfied, the two bodies contact at the grid node I.

(c) Calculate the contact force by Eq. (55) for stick contact, by Eq. (58) for slip contact.

(d) Update the grid nodal momentum for the MPM body by Eq. (53), and update the FE nodal velocity by Eq. (59), FE nodal position by Eq. (47).

5. Loop over all the particles to update their velocities by using

$$v_{ip}^{n+1/2} = v_{ip}^{n-1/2} + \Delta t^n \sum_{I=1}^{n_g} (f_{iI}^n + f_{iI}^{c,n}) N_{Ip}^n / m_I^n \qquad (65)$$

and positions by Eq. (19), respectively.

6. Discard the deformed background grid and define a new regular background grid. Return to step 1 to start a new time step.

7 Numerical examples

7.1 Membrane sphere interaction

Two examples are given here. In the first example, a 50×50 mm^2 elastic membrane falls down at a speed of 50 m/s to a solid elastic sphere with bottom fixed. The thickness of the membrane is 0.1 mm while the radius of the sphere is 15 mm. For the membrane, the Young's modulus is $E = 10 \times 10^3$ MPa, Poisson's ratio $v = 0.3$, and density $\rho = 0.75 \times 10^{-3}$ g/mm^3. For the sphere, the Young's modulus is $E = 70 \times 10^3$ MPa, Poisson's ratio $v = 0.3$, and density $\rho = 2.75 \times 10^{-3}$ g/mm^3.

The discretization of the two bodies is shown in Fig. 5, in which the membrane is modeled by membrane element, while the sphere by MPM particles. The side length of both membrane element and grid cell is 1 mm, and the particle space is 0.5 mm. The coordinates of sphere center are (0, 0, 15), while the membrane are (0, 0, 31). For comparison, this problem is also simulated by FEM using LS-DYNA software.

The time history of the z position of the center (0, 0, 31) and one corner (−25, −25, 31) of the membrane is given in Fig. 6. The results obtained by the presented method and FEM are in good agreement. Furthermore, The snapshots of the falling process obtained by the proposed method at three typical time steps are compare with those obtained by FEM in Fig. 7. It shows that the shapes of the membrane at different time steps obtained by the proposed method are in good agreement with those by FEM.

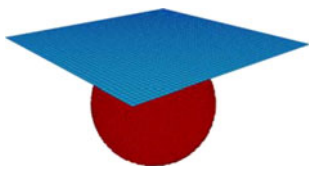

Fig. 5 The discretization of the membrane and sphere

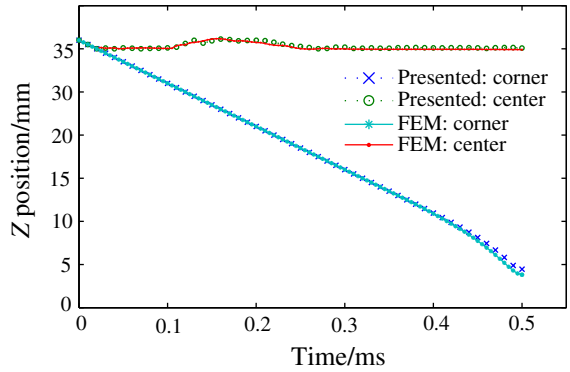

Fig. 6 Time history curve of two points of the membrane

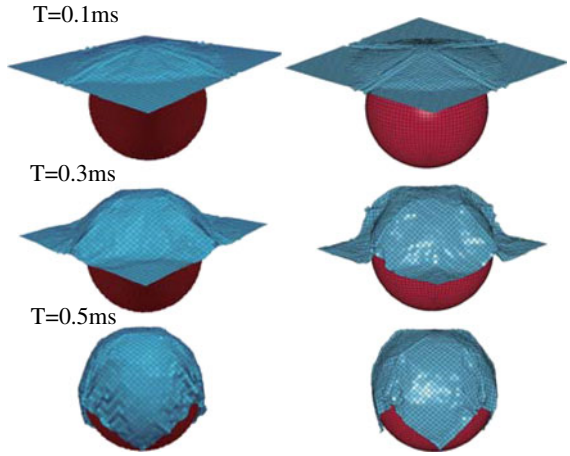

Fig. 7 Snapshots of the falling process

The second example is that a solid sphere falls down at a speed of 10 m/s to a 50×50 mm^2 elastic membrane with four sides fixed. The thickness of the membrane is 0.1 mm while the radius of the sphere is 4.5 mm. Both the membrane and sphere apply the same material constants with the Young's modulus of $E = 70 \times 10^3$ MPa, Poisson's ratio of $v = 0.3$, and density of $\rho = 0.75 \times 10^{-3}$ g/mm^3.

The discretization of the two bodies is shown in Fig. 8, in which the discretization parameters are set as those in the first example. The coordinates of the sphere center are (0, 0, 5.5), while the membrane center are (0, 0, 0). For comparison, this problem is also simulated by FEM.

The time history of the z position of the center (0, 0, 0) of the membrane and top point (0, 0, 10) of the

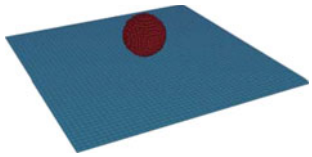

Fig. 8 The discretization of the membrane and sphere

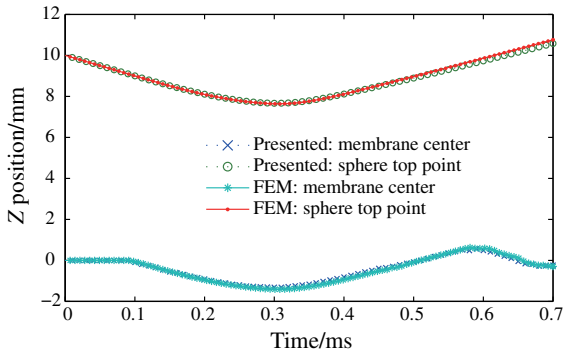

Fig. 9 Time history curves of one point in the membrane and one point on the sphere

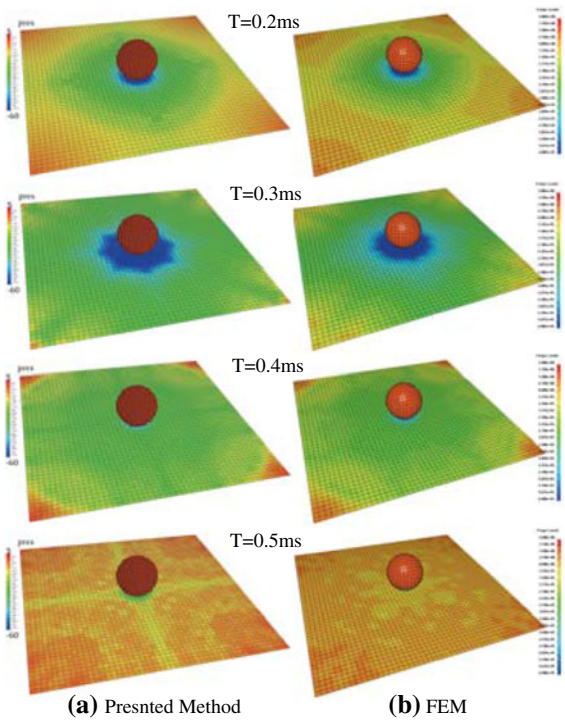

Fig. 10 Snapshots of the falling process

sphere is given in Fig. 9. Besides, the snapshots of the falling process with pressure color obtained by the proposed method at three typical time steps are

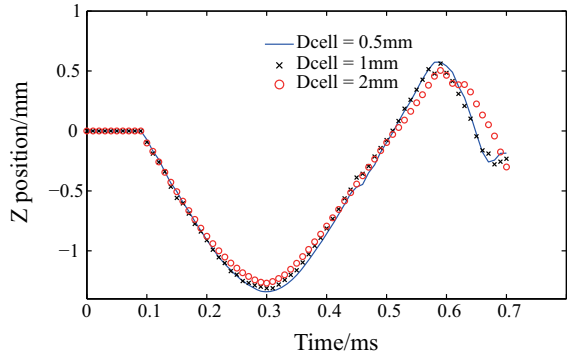

Fig. 11 Time history curves of one point in the membrane

compare with those obtained by FEM in Fig. 10. Both the pressure contour results and the time history curves obtained by the presented method and FEM are in good agreement.

In order to investigate the effect of the cell size on computational results, a convergence analysis is conducted using three models with different cell sizes represented by Dcell. The time history of the z position of the center (0, 0, 0) of the membrane is taken, as shown in Fig.11. The time history curves are more and more close to each other with the decreasing of the cell size.

7.2 Water sphere impact

As shown in Fig. 8, a water sphere of radius $r = 4.5$ mm with initial velocity of 10 m/s moves to a 50×50 mm^2 membrane with four sides fixed. The thickness of the membrane is 0.1 mm. The gap between the water drop and the membrane is $L = 0.5$ mm. The air is neglected, and surface tension model is not applied to this example, which is only used to validate the presented method.

In the simulation, the membrane is modeled by membrane element with density of $\rho = 0.75 \times 10^{-3}$ g/mm^3, Young modulus of $E = 60 \times 10^{-3}$ MPa and the Poisson ratio of $v = 0.3$. The water sphere is modeled by MPM with null material model and Mie-Grüneisen EOS for pressure with material constants listed in Table 1. And the EOS is implemented as follow

$$p = \begin{cases} p_H\left(1 - \frac{\gamma\mu}{2}\right) + \gamma_0 E & \mu \geqslant 0 \\ 0 & \mu < 0 \end{cases} \tag{66}$$

where $p_H = \frac{\rho_0 c_0^2 \mu(1+\mu)}{[1-(s-1)\mu]^2}$, the subscript H refers to the Hugoniot curve, $\mu = \rho/\rho_0 = 1$ indicates the

Table 1 Material constants of water

ρ (kg/m^3)	c_0 (m/s)	s	γ_0
1,000	1,647	1.921	0.1

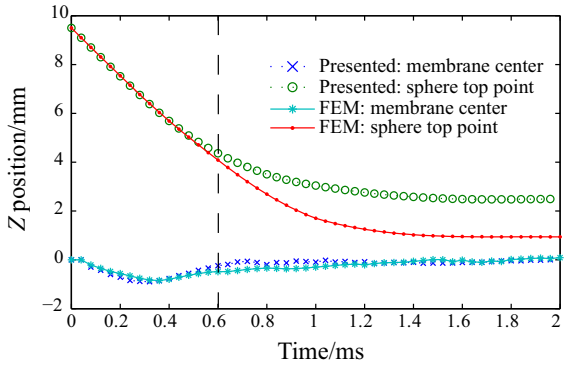

Fig. 12 Time history curves of one point in the membrane and one point on the sphere

compression, and $\gamma = \gamma_0\rho_0/\rho$ is the Grüneisen parameter. The particle space is 0.5 mm, and the side length of both cell and element is 1 mm. For comparison, this problem is also simulated completely by FEM.

The time history of the z position of the center (0, 0, 0) of the membrane and top point (0, 0, 10) of the sphere is given in Fig. 12. Before time 0.6 ms, the curves of both methods agree well with each other, but after that the difference between each other is obvious. Fig. 13 compares the impact process at different time steps between the presented method and FEM. Figure 13a shows that water sphere experiences extreme deformation until to fragmentation, but the water fragmentation phenomenon cannot be modeled by FEM. Therefore, the difference between curves shown in Fig. 13 is mainly because that FEM is unable to model the water sphere fragmentation, as show in Fig. 13.

7.3 Gas expansion

As shown in Fig. 14, a gas block with dimensionless size of 0.9 × 1.9 expands within a membrane. The initial shape of the membrane is a rectangular with dimensionless width of 1, length of 2 and thickness of 0.1. Set the size of both membrane and gas along the z axis as 0.1.

In the simulation, the membrane is modeled by membrane element with density of $\rho = 0.5$, Young

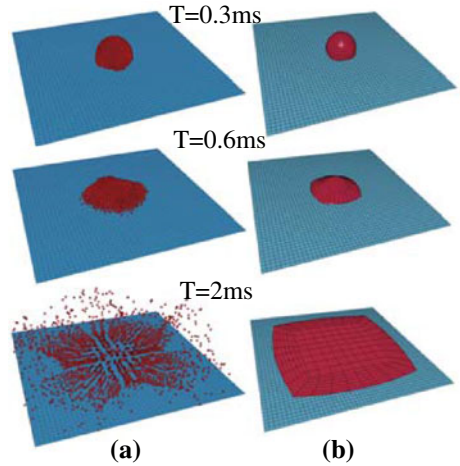

Fig. 13 Snapshots of the water sphere falling process

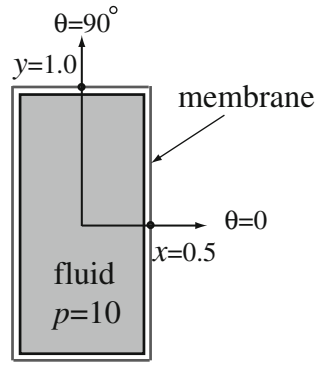

Fig. 14 Initial conditions for the gas block expansion simulation

modulus of $E = 10 \times 10^5$ and the Poisson ratio of $v = 0.3$. The gas body is modeled by MPM with null material model and ideal gas EOS with initial pressure 10. Those material constants are listed in Table 2. By the ideal gas EOS , the gas point pressure is given by

$$p = (\gamma - 1)\frac{\rho}{\rho_0}E, \tag{67}$$

where γ is the ratio of specific heats. In order to damp the membrane oscillations due to the unbalanced forces, the viscosity coefficient μ of the gas is set as 0.1.

Due to the symmetry, one quarter of the model is studied as shown in Fig. 15, with particle space of 0.025, grid cell and the element side length of 0.1.

The radius of the membrane at 0 and 90 degree are shown in Fig. 16. The snapshots of the expansion process are given in Fig. 17. From both Figs. 16 and

Table 2 Material constants of gas

ρ	γ	E_0	μ
1.0	1.4	25	0.1

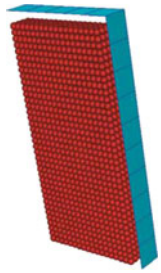

Fig. 15 The discretization of the membrane and gas

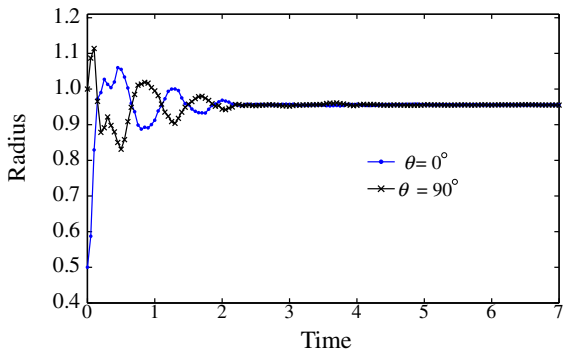

Fig. 16 Radii for membrane

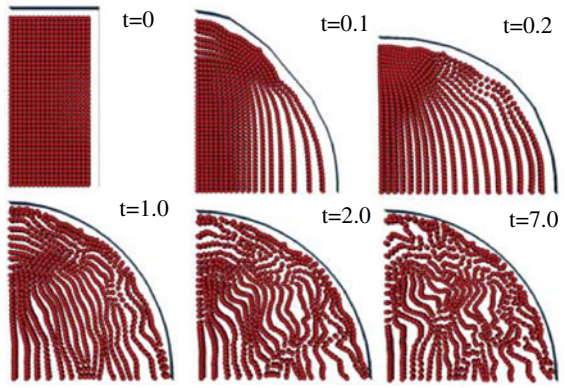

Fig. 17 Snapshots of the gas-membrane expansion

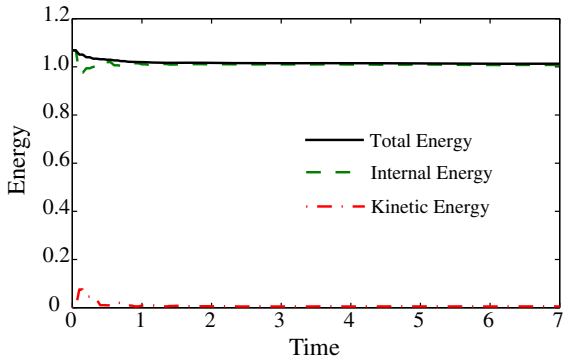

Fig. 18 Energy of the membrane expansion

17, one can find that the membrane oscillates at early time and then is damped to a steady state condition. And the equilibrium shape of the membrane is a circular with the final radius of 0.96. Furthermore, Fig. 18 shows the energy curve, which shows that about 5 % of the energy was lost.

8 Conclusion

In this article, we propose a coupling method to simulate fluid–membrane structure interaction problems. Material point method (MPM) is a Lagrangian particle method, which is suitable for compressible fluids with specific constitutive equation. Due to particles carrying all information, there is no convection terms in momentum equations and easy to track the interface of material. Finite element method (FEM) is a traditional Lagrangian method with high efficiency and accuracy for problems with mild deformation. Therefore, in the proposed method, the fluids are simulated by MPM and the membrane structures by membrane element. The interaction between them is carried out by a contact method implemented on an Eulerian background grid.

Due to the Lagrangian nature of both FEM and MPM, the proposed method has the advantage of allowing an easy definition of the fluid–membrane. The contact between the fluid and membrane structure is also automatically established on background grid when particles and element nodes are close to each other. Numerical examples show that the proposed method is a powerful tool for the fluid–membrane structure interaction problems.

Acknowledgments The research described in this paper was financially Supported by the China Postdoctoral Science Foundation (2013M530040), National Basic Research Program of China (2010CB832701), National Natural Science Foundation of China (11272180), and Tsinghua University Initiative Scientific Research Program.

References

Antoci, C., Gallati, M., Sibilla, S.: Numerical simulation of fluid–structure interaction by SPH. Comput. Struct. **85**, 879–890 (2007)

Bardenhagen, S.G., Brackbill, J.U., Sulsky, D.: The material-point method for granular materials. Comput. Methods Appl. Mech. Eng. **187**(3–4), 529–541 (2000)

Daneshmand, F., Niroomandi, S.: Natural neighbour Galerkin computation of the vibration modes of fluid–structure systems. Eng. Comput. **24**(3–4), 269–287 (2007)

Flanagan, D.P., Belytschko, T.: A uniform strain hexahedron and quadrilateral with orthogonal hourglass control. Int. J. Numer. Methods Eng. **17**, 679–706 (1981)

Gan, Y., Chen, Z., Montgomery-Smith, S.: Improved material point method for simulating the zona failure response in piezo-assisted intracytoplasmic sperm injection. Comput. Model. Eng. Sci. **73**(1), 45–76 (2011)

Gonzalez, D., Cueto, E., Chinesta, F. et al.: A natural element updated Lagrangian strategy for free-surface fluid dynamics. J. Comput. Phys. **223**, 127–150 (2007)

Hallquist, J.O.: LS-DYNA Theoretical Manual. Livermore Software Technology Corporation, Livermore (1998)

Hu, W., Chen, Z.: A multi-mesh MPM for simulating the meshing process of spur gears. Comput. Struct. **81**, 1991–2002 (2003)

Huang, P., Zhang, X., Ma, S., Huang, X.: Contact algorithms for the material point method in impact and penetration simulation. Int. J. Numer. Methods Eng. **85**(4), 498–517 (2011)

Hughes, T.J.R., Liu, W.K., Zimmermann, T.K.: Lagrangian–Eulerian finite element formulation for incompressible viscous flows. Comput. Methods Appl. Mech. Eng. **29**(3), 329–349 (1981)

Idelsohn, S.R., Onate, E., Del Pin, F.: The particle finite element method: a powerful tool to solve incompressible flows with free-surfaces and breaking waves. Int. J. Numer. Methods Eng. **61**(7), 964–989 (2004)

Idelsohn, S.R., Marti, J., Limache, A., Onate, E.: Unified Lagrangian formulation for elastic solids and incompressible fluids: application to fluid–structure interaction problems via the PFEM. Comput. Methods Appl. Mech. Eng. **197**(19–20), 1762–1776 (2008)

Lee, C.J.K., Noguchi, H., Koshizuka, S.: Fluid–shell structure interaction analysis by coupled particle and finite element method. Comput. Struct. **85**, 688–697 (2007)

Lian, Y.P., Zhang, X., Liu, Y.: Coupling of finite element method with material point method by local multi-mesh contact method. Comput. Methods Appl. Mech. Eng. **200**, 3482–3494 (2011)

Liu, M.B., Liu, G.R.: Smoothed particle hydrodynamics (SPH): an overview and recent developments. Arch. Comput. Methods. Eng. **17**, 25–76 (2010)

Luo, H.X., Mittal, R., Zheng, X.D., Bielamowicz, S.A., Walsh, R.J., Hahn, J.K.: An immersed-boundary method for flow–structure interaction in biological systems with application to phonation. J. Comput. Phys. **227**(22), 9303–9332 (2008)

Ma, Z., Zhang, X., Huang, P.: An object-oriented MPM framework for simulation of large deformation and contact of numerous grains. Comput. Model. Eng. Sci. **55**(1), 61–87 (2010)

Rafiee, A., Thiagarajan, K.P.: An SPH projection method for simulating fluid–hypoelastic structure interaction. Comput. Methods Appl. Mech. Eng. **198**(33–36), 2785–2795 (2009)

Souli, M., Ouahsine, A., Lewin, L.: ALE formulation for fluid–structure interaction problems. Comput. Methods Appl. Mech. Eng. **190**(5–7), 659–675 (2000)

Sulsky, D., Chen, Z., Schreyer, H.L.: A particle method for history-dependent materials. Comput. Methods Appl. Mech. Eng. **118**(1–2), 179–196 (1994)

Walhorn, E., Kölke, A., Hübner, B., Dinkler, D.: Fluid–structure coupling within a monolithic model involving free surface flows. Comput. Struct. **83**, 2100–2111 (2005)

York, A.R. II, Sulsky, D., Schreyer, H.L.: Fluid–membrane interaction based on the material point method. Int. J. Numer. Methods Eng. **48**, 901–924 (2000)